Correlated electronic structures and the phase diagram of hydrocarbon-based superconductors

2013 New J. Phys. 15 113030

(http://iopscience.iop.org/1367-2630/15/11/113030)

New Journal of Physics
The open access journal for physics

Correlated electronic structures and the phase diagram of hydrocarbon-based superconductors

Minjae Kim[1], Hong Chul Choi[2], Ji Hoon Shim[2,3,4] and B I Min[1,4]

[1] Department of Physics, PCTP, Pohang University of Science and Technology, Pohang 790-784, Korea
[2] Department of Chemistry, Pohang University of Science and Technology, Pohang 790-784, Korea
[3] Division of Advanced Nuclear Engineering, Pohang University of Science and Technology, Pohang 790-784, Korea
E-mail: jhshim@postech.ac.kr and bimin@postech.ac.kr

New Journal of Physics **15** (2013) 113030 (10pp)
Received 13 August 2013
Published 13 November 2013
Online at http://www.njp.org/
doi:10.1088/1367-2630/15/11/113030

Abstract. We have investigated correlated electronic structures and the phase diagram of electron-doped hydrocarbon molecular solids, based on the dynamical mean-field theory. We have found that the ground state of hydrocarbon-based superconductors such as electron-doped picene and coronene is a multi-band Fermi liquid, while that of non-superconducting electron-doped pentacene is a single-band Fermi liquid in the proximity of the metal–insulator transition. The size of the molecular orbital energy level splitting plays a key role in producing the superconductivity of electron-doped hydrocarbon solids. The multi-band nature of hydrocarbon solids would boost the superconductivity through the enhanced density of states at the Fermi level.

[4] Authors to whom any correspondence should be addressed.

Contents

1. Introduction

Since the discovery of high T_C superconductors, the role of the electronic correlation in the superconductivity has been a subject of intensive investigation. While conventional Bardeen, Cooper and Schrieffer (BCS) superconductors such as Nb and MgB_2 have a good metallic nature of Fermi liquid [1, 2], unconventional superconductors such as doped cuprate and iron pnictide show the bad metallic behavior due to their strong electronic correlation [3, 4]. The correlation issue exists in carbon-based π-electron superconductors too. Ca-doped graphite (CaC_6) shows the conventional superconductivity with weak electronic correlation [5, 6], whereas Cs_3C_{60} exhibits the unconventional superconductivity with strong electronic correlation [7, 8].

New π-electron superconductors have been recently discovered in polycyclic aromatic hydrocarbon (PAH)-based molecular solids: K_3picene ($T_c = 18$ K), K_3coronene ($T_c = 15$ K), K_3phenanthrene ($T_c = 5$ K) and $K_3$1,2;8,9-dibenzopentacene ($T_c = 33$ K) [9–12]. These superconductors were also reported to have a strong correlation [13–16]. On the other hand, a similar PAH-based molecular solid, K-doped pentacene, does not have superconductivity, but exhibits only the metal–insulator transition (MIT) behavior [17]. Note that both picene and pentacene are composed of five benzene rings with slightly different arrangements, as shown in figure 1. The different ground states in K-doped picene and K-doped pentacene suggest that the correlation effects come into play distinctly between superconducting and non-superconducting systems.

In this paper, in order to resolve the issue of correlation effects in hydrocarbon-based superconductors, we have investigated their electronic structures systematically, employing the dynamical mean-field theory (DMFT). Based on the ground state electronic structures, we have constructed the phase diagram of hydrocarbon molecular solids as functions of the doping and relevant energy parameters including the Coulomb correlation, the Hund coupling and the molecular-orbital (MO) energy level splitting. Our studies reveal that hydrocarbon-based superconductors belong to the multi-band Fermi liquid system, while non-superconducting K-doped pentacene belongs to the single-band system in the proximity of the MIT. Further, we have shown that the energy level splitting between LUMO + 1 and LUMO (lowest unoccupied MO) plays a key role in the superconductivity of electron-doped hydrocarbon molecular solids.

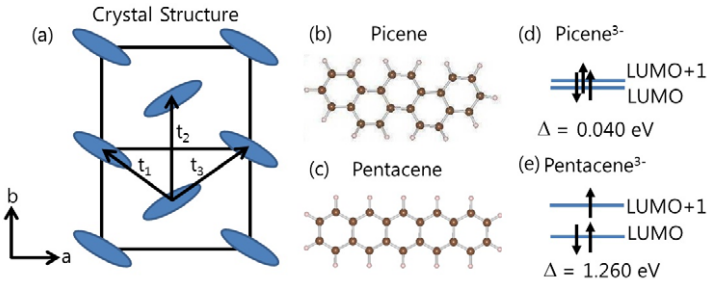

Figure 1. (a) Crystal structure of picene and pentacene solids. Blue ellipses represent picene or pentacene molecular units shown in (b) and (c). t_1, t_2 and t_3 are hopping amplitudes along each direction. (b) Molecular structure of picene. (c) Molecular structure of pentacene. (d) MO energy levels and occupation of electrons for picene^{3-} solid. (e) The same for pentacene^{3-} solid. Note that the energy level splitting (Δ) between LUMO + 1 and LUMO for picene solid ($\Delta = 0.040$ eV) is much smaller than that of pentacene solid ($\Delta = 1.260$ eV).

2. Methods

Both picene and pentacene solids have layered crystal structures, as shown in figure 1(a). Picene molecule has an arm-chair type structure (figure 1(b)), while pentacene molecule has a linear arrangement of benzene rings (figure 1(c)). The difference in molecular structures produces the different electronic structures in three electron-doped picene (picene^{3-}) and pentacene (pentacene^{3-}). As shown in figures 1(d) and (e), the energy level splitting Δ between LUMO + 1 and LUMO of picene solid ($\Delta = 0.04$ eV) is much smaller than that of pentacene solid ($\Delta = 1.26$ eV). Because the bandwidth of each orbital in both molecular solids is $\sim$0.25 eV, picene^{3-} has the occupation of three electrons on nearly two-fold degenerate orbitals [13, 15, 18], whereas pentacene^{3-} has one electron on the single LUMO + 1 orbital that is far separated from the lower LUMO.

The correlation effects in electron-doped hydrocarbon solids are dealt with by the following two-band Hubbard model Hamiltonian:

$$H = H_0 + H_{\mathrm{I}} = \sum_{l,m,\mathbf{R},\sigma} t_{l,m,\mathbf{R}} c^{\dagger}_{l,\mathbf{R},\sigma} c_{m,\mathbf{0},\sigma} + H_{\mathrm{I}}, \tag{1}$$

where H_0 and H_{I} are non-interacting and interacting Hamiltonians of doped electrons, respectively. Here $t_{l,m,\mathbf{R}}$ corresponds to the hopping from (0, m) to ($\mathbf{R}$, l), where 0 and $\mathbf{R}$ represent sites, m and l represent the MOs. We have determined $t_{l,m,\mathbf{R}}$, using the downfolding scheme of Kohn–Sham orbitals in the maximally localized Wannier function (MLWF) basis [19, 20][5]. Kohn–Sham orbitals were obtained in the generalized gradient approximation (GGA), by employing the full-potential augmented plane wave band method [21] implemented in WIEN2k package [22]. For electron-doped systems, we have utilized the rigid band approximation due to the absence of experimental crystal structures. We have employed experimental crystal structures for undoped picene and pentacene [23, 24]. We have confirmed

[5] MLWF provides lower and upper Wannier functions, which are $\frac{1}{\sqrt{2}}(\psi_{\mathrm{LUMO+1}} + \psi_{\mathrm{LUMO}})$ and $\frac{1}{\sqrt{2}}(\psi_{\mathrm{LUMO+1}} - \psi_{\mathrm{LUMO}})$ [18, 20]. We applied the unitary transform to obtain Hamiltonian H_0 with LUMO + 1 and LUMO basis.

Table 1. Hopping amplitudes $t_{l,m,\mathbf{R}}$ (in meV) determined from the *ab initio* band structures of picene and pentacene solids, where l and m represent the MOs, and $\mathbf{R}$ represents the hopping direction in the lattice. Subscript 1, 2 and 3 represent the hopping directions as shown in figure 1, and c represents the direction normal to ab plane.

	$t_{L+1,L,0}$	$t_{L+1,L+1,1}$	$t_{L,L,1}$	$t_{L+1,L+1,2}$	$t_{L,L,2}$
Picene	−10	40	−40	−30	−50
Pentacene	0	60	70	−10	−30
	$t_{L+1,L+1,3}$	$t_{L,L,3}$	$t_{L+1,L+1,c}$	$t_{L,L,c}$	$t_{L+1,L,c}$
Picene	−20	−20	0	0	20
Pentacene	−30	−60	−10	−10	0

that the structure optimization in the GGA does not change the original undoped crystal structures much. The obtained hopping parameters $t_{l,m,\mathbf{R}}$ are provided in table 1.

H_{I} is given approximately by

$$H_{\mathrm{I}} = U \sum_{m,\mathbf{R}} n_{m,\mathbf{R},\uparrow} n_{m,\mathbf{R},\downarrow} + U' \sum_{m>l,\mathbf{R},\sigma} n_{m,\mathbf{R},\sigma} n_{l,\mathbf{R},\bar{\sigma}} + (U' - J) \sum_{m>l,\mathbf{R},\sigma} n_{m,\mathbf{R},\sigma} n_{l,\mathbf{R},\sigma}, \tag{2}$$

where U, U' and J are intra-, inter-orbital Coulomb correlation and Hund interaction parameters, respectively. We considered here the rotationally symmetric interaction, so that $U_{\mathrm{LUMO+1}} \sim U_{\mathrm{LUMO}}$ and $U' \sim U - 2J$ [15]. We have solved the above Hamiltonian by carrying out the DMFT calculation [25]. We used the continuous time quantum Monte-Carlo method as an impurity solver [26, 27]. We set temperature at $T = 77\,\mathrm{K}(=6.67\,\mathrm{meV})$, which is low enough to observe the MIT in the phase diagram of hydrocarbon solids [28].

3. Electronic structures of electron doped picene

Figure 2 shows the imaginary part of the obtained Green's function $G(\mathrm{i}\omega_n)$ and the self-energy $\Sigma(\mathrm{i}\omega_n)$ for LUMO + 1 and LUMO of picene^{3-} solid. For $U = 0.45\,\mathrm{eV}$, $\mathrm{Im}\,G(\mathrm{i}\omega_n)$'s of both LUMO + 1 and LUMO have finite values at $\omega_n = 0$ (ω_n: Matsubara frequency), implying that the densities of states (DOSs) at the Fermi level (E_{F}) are finite for both orbitals. Also $\mathrm{Im}\,\Sigma(\mathrm{i}\omega_n)$'s for both MOs converge to zero in the zero frequency regime, signifying the Fermi liquid nature. Note that the magnitude of $\mathrm{Im}\,\Sigma(\mathrm{i}\omega_n)$ is significantly larger for LUMO + 1 than for LUMO, which reflects that the electronic correlation is stronger for LUMO + 1. In fact, $U = 0.45\,\mathrm{eV}$ corresponds to the value obtained from the first-principles calculation for picene^{3-} solid [15]. So these results indicate that K_3picene solid in its normal state has a two-band Fermi liquid (2FL) nature with clear orbital selective band renormalization.

For $U = 0.65\,\mathrm{eV}$, $\mathrm{Im}\,G(\mathrm{i}\omega_n)$'s near $\omega_n = 0$ appear to be finite for both LUMO + 1 and LUMO, but that for LUMO has a negative slope. From the derivative of $\mathrm{Im}\,G(\mathrm{i}\omega_n)$ near $\omega_n = 0$ one can distinguish between the metallic and the insulating phases as shown in previous literatures [29, 30]. We consider that the positive (negative) derivative illustrates the metallic (insulating) electronic structure. Accordingly, only the LUMO + 1 band has non-zero DOS at E_{F}.

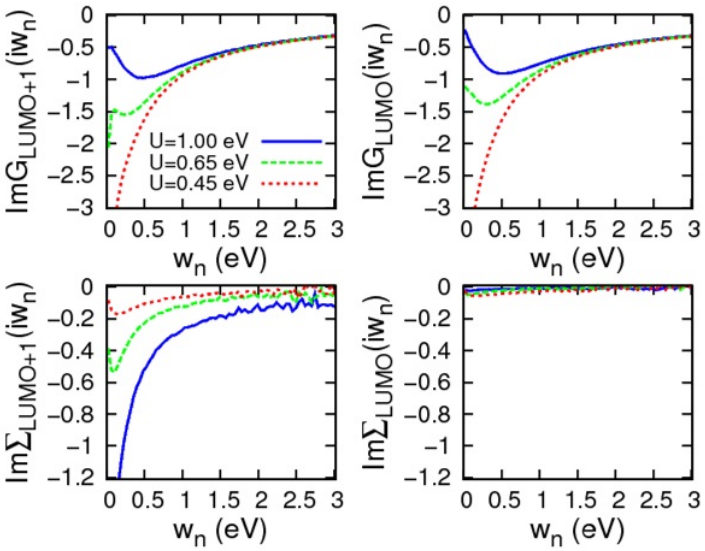

Figure 2. Imaginary Green's functions $G(\mathrm{i}\omega_n)$ and self energies $\Sigma(\mathrm{i}\omega_n)$ of LUMO + 1 and LUMO for picene^{3-} solid ($J = 0.05$ eV and $\Delta = 0.04$ eV). Red (dotted), green (dashed) and blue (solid) lines are for $U = 0.45$, 0.65 and 1.00 eV, respectively.

The behaviors of Im $G(\mathrm{i}\omega_n)$ and Im $\Sigma(\mathrm{i}\omega_n)$ of LUMO + 1 for $U = 0.65$ eV reflect that the system belongs to the narrow single-band Fermi liquid state. For $U = 1.0$ eV, both Im $G(\mathrm{i}\omega_n)$'s are vanishing at $\omega_n = 0$, implying that DOSs at E_F are zero for both LUMO + 1 and LUMO. Im $\Sigma(\mathrm{i}\omega_n)$ at $\omega_n = 0$ diverges for LUMO + 1, indicating that the system has the Mott insulating state with hole–orbital disproportionation nature at LUMO + 1. Namely, the hole–orbital nature changes from the mixture of LUMO and LUMO + 1 to the single LUMO + 1 (see the inset of figure 5).

4. Phase diagrams of electron doped picene and pentacene

Figure 3 shows the ground states of picene and pentacene solids depending on the doping N and the U value. We have obtained the ground states by following the steps in figure 2. As mentioned above, picene^{3-} solid, which has $U = 0.45$ eV, belongs to the 2FL state[6]. This feature reveals that the superconductivity in three electron-doped picene, such as K_3picene and $Ca_{1.5}$picene, emerges from the multi-band Fermi liquid state. If we increase U further for picene^{3-}, the single-band (LUMO + 1) Fermi liquid state is realized at $U = 0.625$ eV, and the Mott insulating state at $U = 0.90$ eV. In the DMFT calculation, Ruff *et al* [16] used $U = 1.6$ eV, which was estimated from the empirical cavity method for the screening of electronic correlation [14]. This U value is considerably larger than $U = 0.45$ eV obtained from the first-principles calculation [15]. That is why Ruff *et al* obtained the Mott insulating state for K_3picene in contrast to our result. Nevertheless, the occurrence of the MIT for large U is consistent between two.

[6] Here U is corresponding to an effective Coulomb interaction that is given by $\bar{U} - \bar{V}$ in [15], where $\bar{U}$ and $\bar{V}$ represent on-site and nearest neighboring Coulomb interactions, respectively.

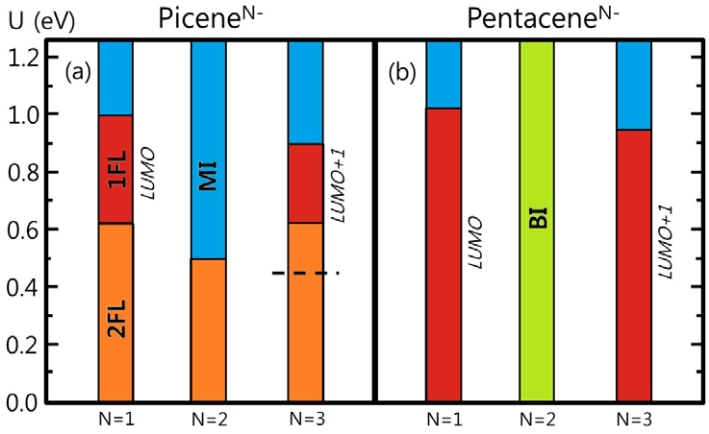

Figure 3. (a) Ground states of picene solid ($J = 0.05$ eV and $\Delta = 0.04$ eV) with variations of doping ($N = 1$, 2, and 3) and Coulomb interaction (U). (b) Ground states of pentacene solid ($J = 0.05$ eV and $\Delta = 1.26$ eV). 1FL, 2FL, BI and MI stand for one-band Fermi liquid, two-band Fermi liquid, band insulator and Mott insulator, respectively. Dashed line for picene^{3-} corresponds to the U value obtained from the first-principles calculation [15].

Similarly to picene^{3-}, picene^{1-} solid also shows the phase transition upon increasing U, from the two-band to the one-band (LUMO) Fermi liquid state, and then to the Mott insulating state. In the case of picene^{2-}, due to the finite Hund coupling J ($= 0.05$ eV), the system for small U remains as a 2FL with the high-spin configuration. With increasing U, the phase transition occurs directly from the 2FL to the Mott insulating state. If one takes into account the non-rigidity of band structures arising from the hybridization with cations in K- or Ca-doped picene, the electronic correlation effect would be further reduced with respect to the above rigid band case [20]. Then K_3picene and $Ca_{1.5}$picene would have more stable 2FL nature in their normal states. If the K doping level is biased from the integer value, the correlation effect would be not so significant as for the integer doping case. As a result, one would obtain the stable 2FL state for the non-integer doping case too. However, in the case of non-integer doping, the disorder effect is expected to become important. In fact, the insulating nature in superconducting $K_x$picene ($x = 3.1$, 3.5) observed above T_C was explained by the granular-metal-like behavior, which would be attributed to the disorder effect [31].

Noteworthy in figure 3(b) is that the ground state of pentacene^{3-} is very different from that of picene^{3-}. Due to the much larger Δ value in pentacene, both pentacene^{3-} and pentacene^{1-} solids exhibit the transition from the single-band Fermi liquid to the Mott insulator, like a single-band half-filled system. On the other hand, pentacene^{2-} has the low-spin state due to large Δ, and so only the band insulating state is realized. The findings in figure 3 manifest that different Δ's of picene and pentacene play key roles in producing the different phases. Also the high-spin and the low-spin configurations of picene^{2-} and pentacene^{2-} suggest that the Hund coupling J affects the phase diagram.

5. Quasi-particle residue Z of electron doped picene with variations of Δ, J and U

Figure 4 presents the quasi-particle residue Z for picene^{3-} solid with the variation of Δ and J. The quasi-particle residue Z is obtained from $Z = (1 - \frac{\mathrm{Im}\,\Sigma(\mathrm{i}w_o)}{w_0})^{-1}$, where w_0 is the

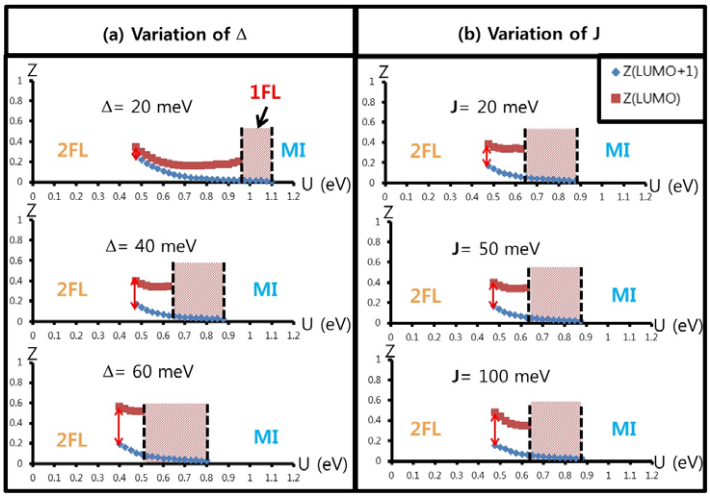

Figure 4. (a) Quasi-particle residue Z's of LUMO + 1 and LUMO versus U for picene^{3-} solid with variation of Δ ($J = 50$ meV). (b) The same for picene^{3-} solid with variation of J ($\Delta = 40$ meV). Red arrow denotes the difference of Z's between LUMO + 1 and LUMO.

lowest Matsubara frequency [29]. With increasing Δ, the following features are observed in figure 4(a): (i) the larger difference of Z's between LUMO + 1 and LUMO, (ii) the wider single-band (LUMO + 1) Fermi liquid regime, and (iii) the reduced critical U for the MIT. The above observations indicate that just a small enhancement of Δ would induce the single-band Fermi liquid state in picene^{3-} solid, and thereby suppress the superconductivity. This sensitive dependence of the electronic structure of picene^{3-} upon variation of Δ explains different experimental electronic structures of K_3picene solid depending on the preparation condition [16, 31–33]. As shown in figure 4(b), the larger J also yields the larger difference of Z's between LUMO + 1 and LUMO. But the single-band Fermi liquid regime and the critical U value for the MIT do not change much. Lager difference of Z's between two MOs implies that the inter-orbital fluctuation becomes suppressed. Therefore figure 4 indicates that the larger Δ induces the orbital disproportionation, and the larger J suppresses the inter-orbital fluctuation [34].

6. Phase diagram of electron doped hydrocarbon-based solid

Figure 5 presents the overall phase diagram of hydrocarbon^{3-} solids as functions of U and Δ. The ground state of picene^{3-} solid is the 2FL. In contrast, the ground state of pentacene^{3-} solid is the single-band Fermi liquid or the Mott insulator depending on U value[7]. This difference is the reason why picene^{3-} is superconducting, while pentacene^{3-} is non-superconducting. With the enhancement of Δ, the system changes from the three electron-doped two-orbital system to the effective one electron-doped one-orbital system. Due to the degeneracy in the two-orbital system, the effective band-width becomes larger ($W_{\rm eff} \sim 1.41$ W), and accordingly, the critical U value for the MIT should be enhanced. The finite J also reduces the correlation strength for the two-orbital system by $3J$ ($\sim$0.6 W) [34]. As a result, the critical U/W value for

[7] First-principle result of U for pentacene^{3-} is not available. The range of U in figure 5 corresponds to that in-between the first-principles [15] and the empirically calculated U [13] for picene^{3-}.

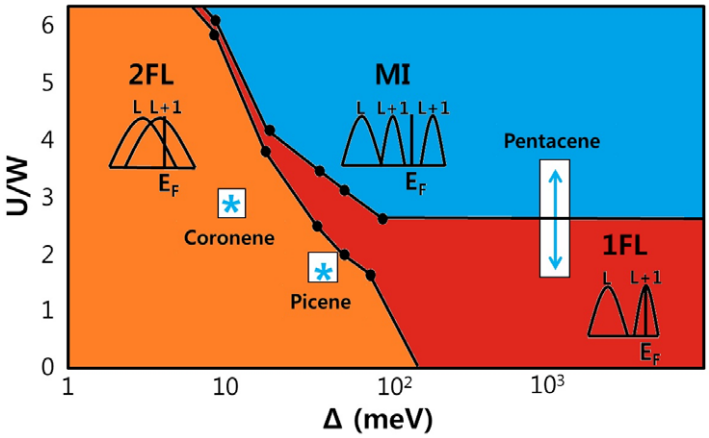

Figure 5. Phase diagram of hydrocarbon^{3-} solids with respect to Coulomb correlation U and MO level splitting Δ. Positions of picene^{3-}, coronene^{3-} and pentacene^{3-} solids are marked in the phase diagram. Inset diagram represents the schematic DOS of each phase. In the MI regime, the hole–orbital disproportionation nature is realized. Here, W is the band-width of the single-orbital crossing E_F. Since W would depend on materials and their crystal structures, we considered U/W as a parameter instead of U.

the MIT in the small Δ limit (2FL) would be almost two times larger than that in the large Δ limit (one band Fermi liquid (1FL)), as shown in figure 5. The ground states of K_3coronene and K_3phenanthrene in their normal states are also the 2FLs, with three doped electrons occupying nearly degenerate LUMO and LUMO + 1. On the other hand, 1,2;8,9-dibenzopentacene has a large energy splitting between LUMO and LUMO + 1, but nearly degenerate LUMO + 1 and LUMO+2 [35]. Hence $K_3$1,2;8,9-dibenzopentacene has one electron on the nearly degenerate LUMO + 1 and LUMO + 2. This situation is similar to that of picene^{1-} in figure 3(a).

Dopant-induced structural deformation and hybridization are to be reflected in the variation of Δ and U/W in figure 5. For example, the total bandwidth of K_3picene is enhanced with respect to that of undoped picene, from ∼0.35 to ∼0.60 eV [20]. As a result, the position of K_3picene would be further lowered from that of picene^{3-} in the phase diagram of figure 5.[8] Also, the effective degeneracy was shown to depend on packing of the crystal structure. According to local-density approximation band calculations [20, 36], out of four near-E_F bands of LUMO + 1 and LUMO from two picene molecules in K_3picene, three bands intersect E_F in a system with closely packed structure, while two bands intersect E_F in a system with more loosely packed structure. Therefore the phase diagram of figure 5 demonstrates that the superconductivity in hydrocarbon-based superconductors commonly emerge from the multi-band Fermi liquid state with good metallic nature. This feature supports the conventional phonon-mediated BCS mechanism rather than other exotic mechanisms for the superconductivity of hydrocarbon-based molecular solids [37–41], despite that they have U/W larger than one. Recent report on

[8] There are several metastable structures for K_3picene [16, 20, 31–33]. Determination of Δ and U/W for each metastable structure would be an interesting future problem. Large Δ and U/W due to the more loosely packed structure of the metastable phase would induce the Mott insulating state with Curie–Weiss susceptibility behavior.

K-doped 1,2;8,9dibenzopentacene corroborates that the conventional BCS theory accounts for its highest $T_c = 33$ K in hydrocarbon-based superconductors [42].

The underlying superconducting mechanism in hydrocarbon-based superconductors needs further investigation, but it is evident that the superconductivity would be boosted up by the enhanced DOS at E_F due to their multi-band Fermi liquid nature [38]. Our phase diagram indicates that small U/W and Δ are key factors for the emergence of superconductivity in hydrocarbon-based molecular solids. Thus the superconductivity is preferentially to be searched for in closely packed hydrocarbon-based molecular solids that have small U/W and Δ.

7. Conclusion

We have investigated the electronic structures of electron-doped hydrocarbon solids based on the DMFT calculations, and constructed the phase diagram with respect to the Coulomb correlation U, the doped electrons N, the Hund coupling J and the MO energy level splitting Δ. We have shown that the superconductivity in hydrocarbon solids commonly emerges from the multi-band Fermi liquid state. This is in contrast to the case of non-superconducting pentacene, which has the effective single-band Fermi liquid state in the proximity of the MIT. The size of MO energy level splitting plays an important role in determining the ground states of hydrocarbon solids. Our results demonstrate that the multi-band nature in hydrocarbon solids is essential to boost the superconductivity through the enhanced DOS at E_F. It is thus suggested that higher T_C superconductors need to be searched for in the more closely packed molecular solids with the multi-band nature at E_F.

Acknowledgments

Discussions with Ki-Seok Kim and Beom Hyun Kim are gratefully acknowledged. This work was supported by the National Research Foundation of Korea (grant numbers 2009-0079947, 2010-0006484 and R32-2008-000-10180-0).

References

[1] Bauer R, Schmid A, Pavone P and Strauch D 1998 *Phys. Rev.* B **57** 11276
[2] Choi H J, Roundy D, Sun H, Cohen M L and Louie S G 2002 *Nature* **418** 758
[3] Lee P A, Nagaosa N and Wen X-G 2006 *Rev. Mod. Phys.* **78** 17
[4] Haule K, Shim J H and Kotliar G 2008 *Phys. Rev. Lett.* **100** 226402
[5] Csányl G, Littlewood P B, Nevidomskyy A H, Pickard C J and Simons B D 2005 *Nature Phys.* **1** 42
[6] Lamura G, Aurino M, Cifariello G, Di Gennaro E, Andreone A, Emery N, Hérold C, Marêché J F and Lagrange P 2006 *Phys. Rev. Lett.* **96** 107008
[7] Capone M, Fabrizio M, Castellani C and Tosatti E 2009 *Rev. Mod. Phys.* **81** 943
[8] Ihara Y, Alloul H, Wzietek P, Pontiroli D, Mazzani M and Riccò M 2011 *Europhys. Lett.* **94** 37007
[9] Mitsuhashi R *et al* 2010 *Nature* **464** 76
[10] Kubozono Y *et al* 2011 *Phys. Chem. Chem. Phys.* **13** 16476
[11] Wang X F, Liu R H, Gui Z, Xie Y L, Yan Y J, Ying J J, Luo X G and Chen X H 2011 *Nature Commun.* **2** 507
[12] Xue M, Cao T, Wang D, Wu Y, Yang H, Dong X, He J, Li F and Chen G F 2012 *Sci. Rep.* **2** 389
[13] Kim M, Min B I, Lee G, Kwon H J, Rhee Y M and Shim J H 2011 *Phys. Rev.* B **83** 214510
[14] Giovannetti G and Capone M 2011 *Phys. Rev.* B **83** 134508

[15] Nomura Y, Nakamura K and Arita R 2012 *Phys. Rev.* B **85** 155452
[16] Ruff A, Sing M, Claessen R, Lee H, Tomić M, Jeschke H O and Valentí R 2013 *Phys. Rev. Lett.* **110** 216403
[17] Craciun M F, Giovannetti G, Rogge S, Brocks G, Morpurgo A F and van den Brink J 2009 *Phys. Rev.* B **79** 125116
[18] Kosugi T, Miyake T, Ishibashi S, Arita R and Aoki H 2009 *J. Phys. Soc. Japan* **78** 113704
[19] Mostofi A A, Yates J R, Lee Y-S, Souza I, Vanderbilt D and Marzari N 2008 *Comput. Phys. Commun.* **178** 685
[20] Kosugi T, Miyake T, Ishibashi S, Arita R and Aoki H 2011 *Phys. Rev.* B **84** 214506
[21] Weinert M, Wimmer E and Freeman A J 1982 *Phys. Rev.* B **26** 4571
[22] Blaha P, Schwarz K, Madsen G K H, Kavasnicka D and Luitz J 2001 *WIEN2k* (Wien: Technische Universitat Wien)
[23] De A, Ghosh R, Roychowdhury S and Roychowdhury P 1985 *Acta Crystallogr.* C **41** 907
[24] Campbell R B, Robertson J M and Trotter J 1961 *Acta Crystallogr.* **14** 705
[25] Kotliar G, Savrasov S Y, Haule K, Oudovenko V S, Parcollet O and Marianetti C A 2006 *Rev. Mod. Phys.* **78** 865
[26] Haule K 2007 *Phys. Rev.* B **75** 155113
[27] Werner P, Comanac A, de'Medici L, Troyer M and Millis A J 2006 *Phys. Rev. Lett.* **97** 076405
[28] Georges A, Kotliar G, Krauth W and Rozenberg M J 1996 *Rev. Mod. Phys.* **68** 13
[29] Kováčik R, Werner P, Dymkowski K and Ederer C 2012 *Phys. Rev.* B **86** 075130
[30] Fuchs S, Gull E, Troyer M, Jarrell M and Pruschke T 2011 *Phys. Rev.* B **83** 235113
[31] Teranishi K, He X, Sakai Y, Izumi M, Goto H, Eguchi R, Takabayashi Y, Kambe T and Kubozono Y 2013 *Phys. Rev.* B **87** 060505
[32] Mahns B, Roth F and Knupfer F 2012 *J. Chem. Phys.* **136** 134503
[33] Caputo M *et al* 2012 *J. Phys. Chem.* C **116** 19902
[34] de'Medici L 2011 *Phys. Rev.* B **83** 205112
[35] Mahns B, Roth F, König A, Grobosch M, Knupfer M and Hahn T 2012 *Phys. Rev.* B **86** 035209
[36] de Andres P L, Guijarro A and Vergés J A 2011 *Phys. Rev.* B **83** 245113
[37] Gunnarsson O 1997 *Rev. Mod. Phys.* **69** 575
[38] Kato T, Kambe T and Kubozono Y 2011 *Phys. Rev. Lett.* **107** 077001
[39] Casula M, Calandra M, Profeta G and Mauri F 2011 *Phys. Rev. Lett.* **107** 137006
[40] Casula M, Calandra M and Mauri F 2012 *Phys. Rev.* B **86** 075445
[41] Subedi A and Boeri L 2011 *Phys. Rev.* B **84** 020508
[42] Kato T 2013 *J. Phys. Chem.* C **117** 17211